Nano Energy 25 (2016) 225–231

Contents lists available at ScienceDirect

Nano Energy

journal homepage: www.elsevier.com/locate/nanoen

Triboelectric contact surface charge modulation and piezoelectric charge inducement using polarized composite thin film for performance enhancement of triboelectric generators

Yang Hyeog Kwon [a], Sung-Ho Shin [a], Young-Hwan Kim [a], Joo-Yun Jung [b], Min Hyung Lee [c], Junghyo Nah [a,*]

[a] Department of Electrical Engineering, Chungnam National University, Daejeon 34134, Republic of Korea
[b] Department of Nano Manufacturing Technology, Korea Institute of Machinery and Materials, Daejeon 34103, Republic of Korea
[c] Department of Applied Chemistry, Kyung Hee University, Yongin, Gyeonggi, 17104, Republic of Korea

ARTICLE INFO

Article history:
Received 18 February 2016
Received in revised form
2 April 2016
Accepted 2 May 2016
Available online 3 May 2016

Keywords:
Triboelectricity
Ferroelectric polarization
Ceramic-polymer composite

ABSTRACT

We report performance enhancement of triboelectric generators (TEGs) by modulating dielectric permittivity and optimizing the effects from polarized dipoles in the composite thin films, composed of barium titanate nanoparticles (BTO NPs) and polydimethylsiloxane (PDMS). Thanks to BTO's high permittivity and ferroelectric property, the composite thin films provide excellent platforms to examine both permittivity modulation and surface dipole effects on performance of TEGs. Our results show that peak output power density of the TEGs is increased in proportion to *cubic* BTO NP wt% in the composite layer, increasing permittivity of it. More interestingly, both contact surface charge density modulation and piezoelectric charge inducement were achieved by polarized *tetragonal* BTO NPs in the composite layer. By optimizing wt% of *tetragonal* BTO NPs and polarization of the composite layer, the output performance of TEG was greatly improved, generating the output voltage of ~380 V and peak power density of 2.5 mW cm^{-2} with a 10 MΩ load resistance. The work here provides simple performance enhancement methods and offers an insight into the roles of both permittivity-induced and polarized dipole-induced effects on the electrical output of TEGs.

© 2016 Elsevier Ltd. All rights reserved.

1. Introduction

Triboelectric nanogenerators (TEGs), which can harvest energy from various resources in our living environment such as wind [1–3], wave [4–6], raindrops [7–9], and human motions [10–12], have gained great attention thanks to their relatively high output power and simple device structures by comparison to other energy harvesting devices. To date, numerous methods have been adopted and investigated to further improve output performance of TEG. For instance, performance enhancements of TEGs have been reported by using various surface patterning methods [13–20], optimizing triboeletric contact pairs, and chemically functionalizing surface electrification property [21]. More recently, TEG performance enhancement by surface dipoles [22] and permittivity modification [23,24] has been reported. These methods effectively improved performance of TEGs, which can also potentially be integrated with other surface patterning and functionalization techniques for further performance enhancement. However, only few results have been reported to date using these methods [22–24] and further experimental and theoretical investigations are necessary for in-depth understanding.

In this work, we employed $BaTiO_3$ nanoparticles (BTO NPs) to form BTO NPs- PDMS (Polydimethylsiloxane) composite thin films to demonstrate polarized dipole effects and permittivity modulation effect. Thanks to BTO's high permittivity and ferroelectric property, BTO NPs-PDMS composite thin films provide an excellent platform to examine both effects on performance of TEGs. Here, we used two different types of BTO NPs: *cubic* BTO NPs for permittivity modulation and *tetragonal* BTO NPs for surface charge and piezoelectric charge inducement. Our results show that the permittivity modulated TEGs and polarized dipole enhanced TEGs demonstrate 5-fold and 6-fold higher peak output power densities, respectively, by comparison to the TEG without BTO NPs in the composite thin film layer. In particular, the highest peak output power density was achieved by dipole polarization in the composite layer, generating the output voltage of ~380 V and peak power density of ~2.5 mW cm^{-2} with a 10 MΩ load resistance.

* Corresponding author.
E-mail address: jnah@cnu.ac.kr (J. Nah).

http://dx.doi.org/10.1016/j.nanoen.2016.05.002
2211-2855/© 2016 Elsevier Ltd. All rights reserved.

2. Experimental methods

2.1. BTO NPs-PDMS composite thin film TEG

To make BTO NPs-PDMS composite thin film TEG, average size 100 nm *cubic* and average size 200 nm *tetragonal* (U. S. Research Nanomaterials, Inc.) BTO NPs were poured in prepared PDMS (Sylgard 184, Dow Corning) by varying a BTO NP weight ratio (wt%). Mixed solution was stirred with magnetic bar for 10 min for uniform distribution of BTO NPs in the PDMS. The well-distributed BTO NPs-PDMS solution was then poured on PET/ITO film and spin-coated at 2000 rpm for 30 s The solution coated PET was placed in vacuum desiccator at room temperature for 2 h. Finally, the solution-coated PET was cured at 80 °C for 2 h. In case of *tetragonal* BTO NPs-PDMS composite thin film, it was poled at 125 °C while applying an electric field (10 kV cm^{-1}) for 10 h.

2.2. Electrical characterization

The output voltage and current of TEG were measured by using an oscilloscope (Waverunner2 LT 354, Lecroy) and current pre-amplifier (Stanford Research Systems, SR570), respectively. The output characteristics of TEGs were measured while applying periodic force (0.3 MPa, 2 Hz) normal direction to the surface using the custom-made pushing machine. The area of the contact surface is 4 cm^2. The surface charge densities of the TEGs were measured using the electrometer (Keithley 6514) after contact electrification for 500 cycles.

2.3. Optical characterization

The BTO NPs were characterized by using both scanning electron microscope and high resolution Raman spectroscopy (Lab-RAM HR-800 UV-Visible-NIR, HORIBA JOBIN YVON).

3. Results and discussion

In order to investigate the roles of surface dipoles and permittivity modulation effects on the performance of TEGs, two different types of composite thin films were prepared, composed either of *cubic* phase BTO NPs to test permittivity modulation effect or *tetragonal* phase BTO NPs to examine surface dipole effects. As shown in Fig. 1(a) and (b), BTO NPs show significantly different particle sizes and optical properties, where an average size of *tetragonal* BTO NPs is ~200 nm, while *cubic* BTO NPs show an average size less than ~ 100 nm. Here, strong ferroelectricity can be noticed in *tetragonal* BTO NPs due to asymmetric crystal structure. Raman spectrum also reveals that *tetragonal* BTO NPs exhibit good ferroelectric property [Fig. 1(b)]: the obvious peaks of longitudinal (LO) and transverse (TO) modes at 256 cm^{-1} [A_1(TO)], 306 cm^{-1} [E, B_1(TO+LO)], 513 cm^{-1} [E, A_1(TO)], and 715 cm^{-1} [E, A_1(LO)] are consistent with previous reports [25,26]. Using these different BTO NPs, BTO NPs-PDMS composite thin films were prepared as described in Fig. 1(c). First, each type of BTO NPs was poured in liquid phase PDMS and the solution was stirred for uniform NPs distribution. To obtain thin composite layer, the prepared solution was spin-coated on a PET/ITO film at 2000 rpm for 30 s The solution-coated thin film was then placed in vacuum desiccator for 2 h at room temperature (RT) until NPs subside near

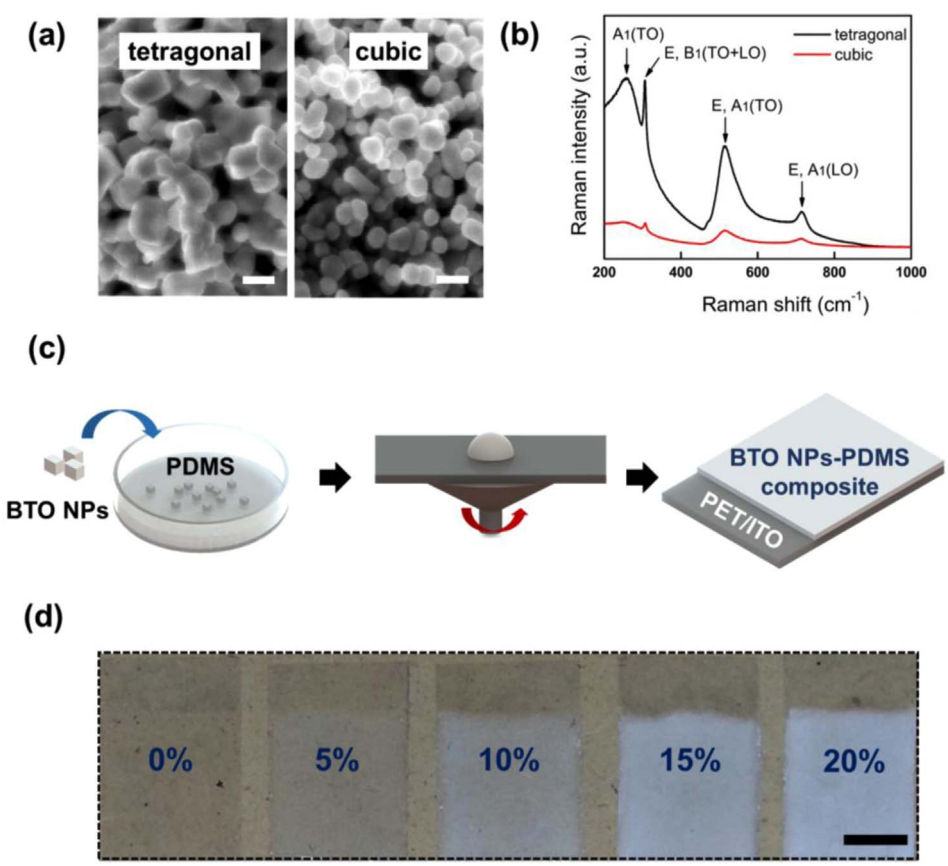

Fig. 1. (a) SEMs of *tetragonal* and *cubic* phase BTO NPs. (Scale bar: 200 nm) (b) Raman spectra of *tetragonal* and *cubic* phase BTO NPs. (c) Schematic representations of the BTO NPs-PDMS composite thin film fabrication process. (d) Optical images of BTO NPs-PDMS composite thin films coated on the ITO-PET substrates. The BTO wt% is varied from 0 to 20%. (Scale bar: 1 cm).

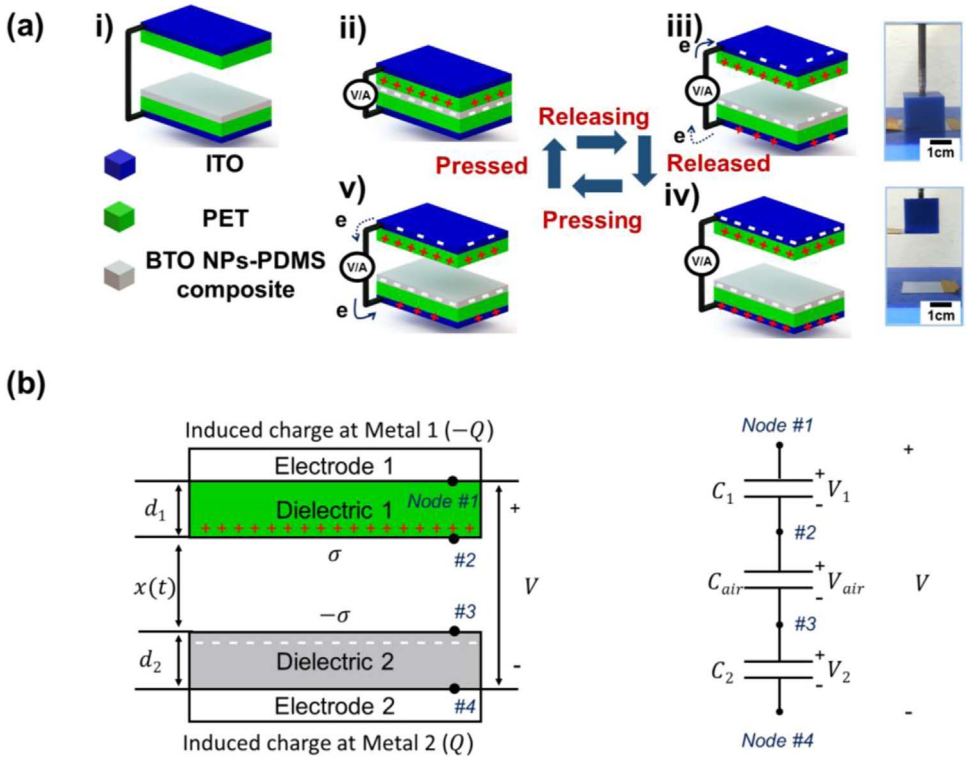

Fig. 2. (a) Schematic representation of TEG output generation mechanism: i) Initial state: no surface charge on both PET and BTO NPs-PDMS composite. ii) Pressed state: inducing positive surface charges on a PET surface and negative surface charges on a BTO NPs-PDMS composite thin film surface originated from their differences in electron affinity. iii) Releasing state: electrical equilibrium state breaks and electrons flow toward the top electrode through external circuit. iv) Released state: electrical equilibrium between each surface and facing electrode. v) Pressing state: electrons start to flow in the opposite direction. (b) Schematic diagram and an equivalent circuit model of the BTO NPs-PDMS composite TEG.

the bottom of the surface due to large density difference between BTO NPs and PDMS [Fig. S1 (Supporting information)]. Finally, BTO NPs-PDMS composite thin films were cured in oven for 2 h at 80 °C. Additionally, the composite thin film containing *tetragonal* NPs was poled under high electric field to align polarization domains of the NPs in PDMS. Fig. 1(d) shows the optical images of the thin films on a PET/ITO substrate with different BTO NPs wt%. Both types of the composite films, either with *cubic* or *tetragonal* BTO NPs, became translucent as the BTO NP weight ratio increases.

Fig. 2(a) demonstrates the schematic representations of generation mechanisms of the TEG. The TEG is consisted of a BTO NPs-PDMS composite layer and a PET counter contact layer. At the initial state, there is no surface charge on both BTO NPs-PDMS composite surface and PET surface [Fig. 2(a)(i)]. As two surfaces are pressed against each other, the surface charge transfer occurs between BTO NPs-PDMS composite layer and PET surface [Fig. 2(a)(ii)]. Since electron affinity of the BTO NPs-PDMS composite is much higher than that of PET, negative charges are induced on the BTO NPs-PDMS composite surface, while positive charges are induced on the PET surface. When two surfaces are separated, charge equilibrium state between two surfaces is broken and electrons at the bottom electrode start to flow through an external circuit toward the top electrode [Fig. 2(a)(iii)]. After two surfaces are fully separated, charge equilibrium state is reached between the electrode and the contacting surface [Fig. 2(a)(iv)]. Lastly, when two surfaces are pressed again each other, charge equilibrium state is broken again and electrons start to flow in the opposite direction [Fig. 2(a)(v)]. Therefore, periodic pressing and releasing motions of TEG generate alternating voltage and current pulses. Fig. 2(b) shows a schematic of TEG and a corresponding equivalent electric circuit model. It consists of two dielectric materials, which have thicknesses and permittivities of (d_1, ε_1) and (d_2, ε_2), respectively, and an identical surface area (S). We assumed constant surface charge density (σ) placed on the dielectric surfaces, inducing the charge (Q) at the facing electrode surfaces. The surface charges on two dielectric surfaces develop potential difference between two dielectric surfaces. Similarly, surface charges on the dielectric surface and induced charges on the electrode surfaces also generate potential difference. Thus, the TEG structure can be modeled as capacitors connected in series and its voltage output can be expressed as the following Eq. (1) [27].

$$V = \frac{\sigma x(t)}{\varepsilon_0} - \frac{Q}{S\varepsilon_0}\left(\frac{d_1}{\varepsilon_1} + \frac{d_2}{\varepsilon_2} + x(t)\right) \quad (1)$$

In Eq. (1), surface charge density (σ) on the dielectric surfaces, induced charges (Q) on the electrodes, and permittivity of dielectric materials are the key factors related with output performance of the TEG. In this work, we note that permittivity modulation effect was investigated using *cubic* BTO NPs-PDMS composite thin films and surface dipole effects on surface and induced charge density were examined using polarized *tetragonal* BTO NPs-PDMS composite thin films.

Output performance enhancement of the TEG by permittivity modulation was first investigated [Fig. 3(a)]. Specifically, output voltage and current of the TEGs, containing different wt% of *cubic* BTO NPs in the composite thin film, were examined. The peak output voltage and current of the TEG without BTO NPs were ~150 V and ~12 μA cm^{-2}, respectively. The output performance was gradually enhanced as the wt% of *cubic* BTO NPs in the composite was increased to 20 wt%. At 20 wt% BTO NPs in the composite film, peak output voltage and current were reached ~300 V and ~30 μA cm^{-2}, respectively, which correspond to ~5-fold higher peak output power density compared with that of the TEG without BTO NPs. This enhancement is originated from

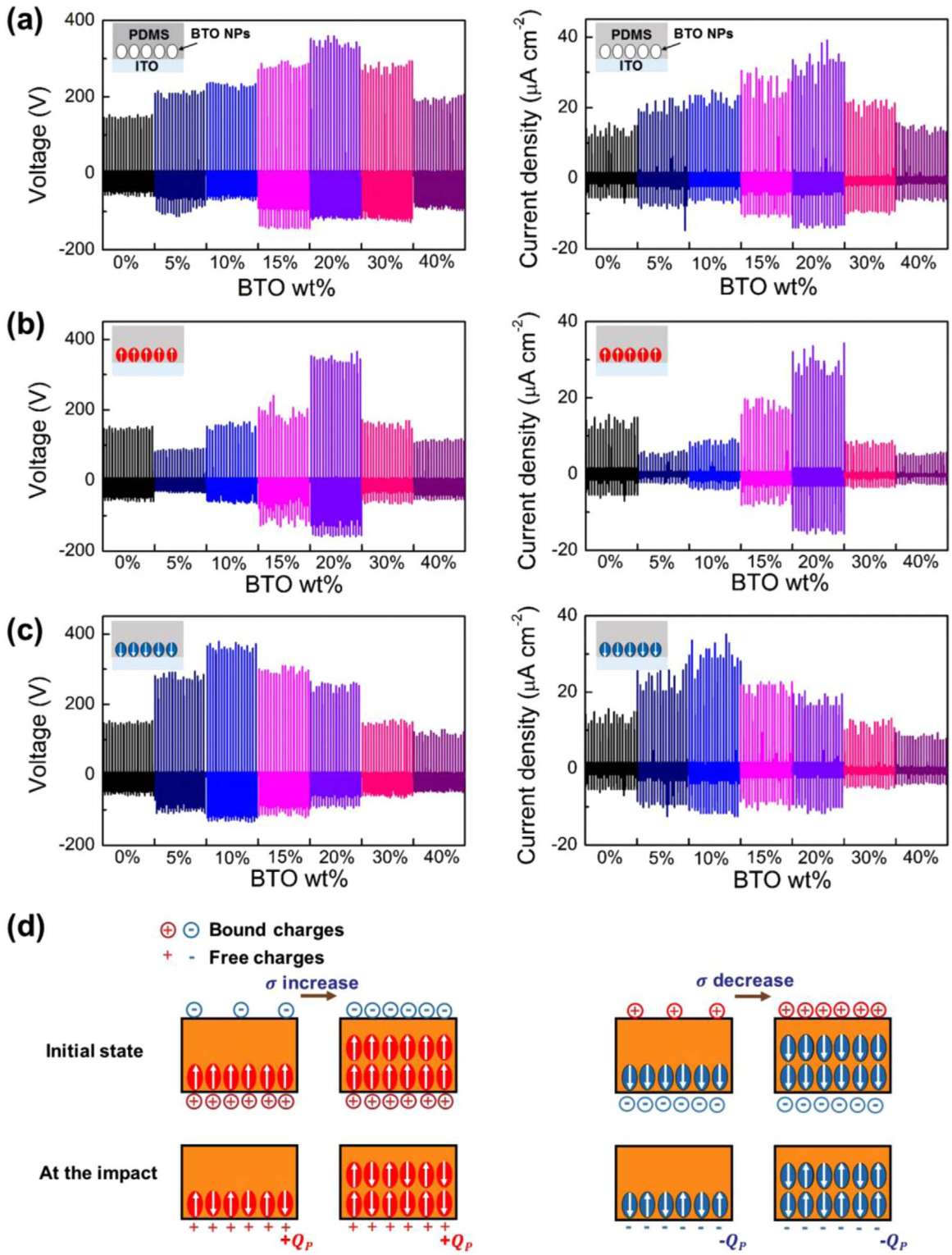

Fig. 3. (a) Output voltage and current of the TEGs with different *cubic* phase BTO NPs wt% in the composite thin film. (b, c) Output voltage and current of the TEG with different wt% of *tetragonal* phase BTO NPs in the composite thin film. (Insets) the directions of arrow indicate polarization directions: (b) upward polarization and (c) downward polarization. (d) Surface charge density modulation and piezoelectric charge inducement by polarized dipoles in the composite. At the initial state, in downward (upward) polarized composite, positive (negative) charges are induced on the top dielectric surface and negative (positive) bound charges are induced on the bottom electrode. As the BTO wt% increases, the induced surface charges on the dielectric surface increases as the polarized dipoles are located close to the surface, decreasing or increasing triboelectrically induced surface charge density. At the contact (impact), the charges on the dielectric surface are neutralized by the counter surface and bounded charges on the electrode are released, generating Q_P or $-Q_P$.

permittivity increase in the BTO NPs-PDMS composite thin film [Fig. 3(d), Fig. S2]. As described in Eq. (1), the permittivity (ε_2) increase leads to output voltage increase of TEG. The validity of output signal was confirmed by measuring the TEG under a reverse-connection mode [Fig. S3]. As the wt% of BTO NPs further increases to 40 wt%, the output voltage and current were rather

reduced due to exposed NPs on the PDMS surface [Fig. S4]. Although the permittivity of the composite layer increases in proportion to the wt% of BTO NPs, however, effective contact surface area is rather reduced when the wt% of NPs exceeds 30 wt%.

Next, TEGs, composed of polarized *tetragonal* BTO NPs-PDMS composite thin films, were investigated to understand polarized dipole effects. Output performance of the TEGs was examined while varying wt% of *tetragonal* BTO NPs and their dipole polarization directions in the composite film [Fig. 3(b) and (c)]. The results in Fig. 3(b and c) clearly show different tendencies in comparison with those in Fig. 3(a), affected by both BTO NPs' wt% and dipole polarization directions. Fig. 3(b) shows the results of the TEG with upward polarized composite films, containing different wt% of BTO NPs inside the composite. When the wt% BTO NPs in the composite is 5 wt%, both output voltage and current were rather decreased [Fig. 3(b)]. As the wt% of BTO NPs reaches 20 wt%, the outputs of the TEG were rapidly increased to ~350 V and ~30 μA cm^{-2}, respectively. However, the outputs were rapidly decreased when the wt% of BTO NPs exceeds 30 wt%. On the other hand, when BTO NPs in the composite thin film are polarized downward, different patterns of output voltage and current were displayed. The output voltage and current density of ~280 V and ~22 μA cm^{-2} were respectively obtained in the TEG with 5 wt% *tetragonal* BTO NPs composite film, which are much higher values compared with those of the TEG with the same wt% BTO NPs polarized opposite direction. The output performance was enhanced until the wt% of BTO NPs reaches 10 wt%, exhibiting output voltage and current density up to ~380 V and ~30 μA cm^{-2}, respectively [Fig. 3(c)]. As the wt% of BTO NP further increases, both output voltage and current were decreased. As described, performance degradation above 30 wt% in both cases is attributed to exposed NPs on the PDMS surface, which is more obvious for the composite with *tetragonal* BTO NPs due to their relatively larger sizes by comparison to *cubic* BTO NPs. Fig. 3(d) explains the roles of polarized dipoles on the output performance of TEGs. At the initial state, due to remnant polarization of BTO NPs inside PDMS after high voltage poling process, bound charges are induced on both top dielectric surface and bottom electrode to maintain charge neutrality. As shown in Fig. S1, the BTO NPs are predominantly located near the bottom electrode due to their high density compared with PDMS. Thus, more charges are bounded on the bottom electrode than the top dielectric surface [Fig. 3(d) top]. Here, since there is no electrode deposited on the top dielectric surface, charges adsorption will occur on the dielectric surface to maintain electroneutrality, negatively or positively charging the contact surface. Thus, surface charge state will be modulated differently depending on the polarization direction and wt% of BTO NPs in the composite layer, affecting triboelectrically induced surface charge density. At the moment of contact between the PET and the composite layer [Fig. 2(a, ii)], triboelectrically induced negative charges on the dielectric surface will be neutralized by counter charges on the PET surface and the polarization will instantaneously disappear, releasing the bound charges on the electrode [Fig. 3(d) bottom]. Therefore, piezoelectrically generated charge (Q_P) is developed only when the two surfaces are contacted. As the wt% of BTO NPs increases, more charges are induced on the contact surface: negative charges for upward polarization and positive charges for downward polarization. Consequently, net negative triboelectric surface charge density (σ) on the PDMS surface can be increased by upward polarization or decreased by downward polarization. This becomes more obvious as the wt% of BTO NPs increases in the composite. For the TEGs with upward polarized films, the contact surface charge density (σ) will be gradually increased in proportion to the wt% of BTO NPs since more negative charges are induced on the surface by polarized dipoles. Piezoelectrically induced charge ($+Q_p$) will also be increased as the wt% of BTO NPs increases but will have a saturated value once the BTO NPs cover the sufficient electrode surface. For experimental verification, we directly measured the surface charge densities of the composite film with different wt% of upward polarized BTO NPs [Fig. S5]. Up to 10 wt% of BTO NPs in the composite layer, surface charge density was not obviously changed since the NPs are mainly located close to the bottom electrode and thus not strongly coupled to the dielectric surface. However, $+Q_P$ is expected to continuously increase until the wt% of BTO NPs in the composite reaches 10 wt%. Thus, similar or even smaller outputs compared with 0 wt% case can be anticipated using Eq. (1). As the wt% of BTO NPs is increased to 20 wt% in the composite, the surface charge density was two-fold increased by comparison to the initial value. Above 30 wt% BTO NPs in the composite, the NPs are exposed on the PDMS surface and triboelectric surface charge density (σ) is rapidly reduced, decreasing output voltage and current of the TEG. The output trends of TEG fabricated with downward polarized composite can be similarly explained. With inclusion of downward polarized BTO NPs in the composite, positive bound charges are induced on the dielectric surface and negative bound charges on the bottom electrode at the initial state [Fig. 3(d) right]. At the moment of the contact between PET and PDMS surfaces, negative charges on the dielectric surface will be neutralized by counter charges on the PET surface and the polarization will instantaneously disappear, releasing the bound charges on the electrode. Similar to the TEG with upward polarized film, there exists minimal effect on triboelectric surface charge density until the wt% BTO NPs in the composite reaches 10 wt%. On the other hand, piezoelectrically induced negative charge ($-Q_p$) is expected to continuously grows until the saturation value is reached. Thus, based on the Eq. (1), total output voltage can be increased only when the wt% of BTO NPs in the composite is low. However, as the wt% of BTO NPs increases, surface charge density (σ) on the dielectric surface will be continuously reduced because the polarized dipoles are more strongly coupled to the dielectric surface and induces positive charges, reducing σ. As a result, total output voltage will be reduced. Indeed, measured surface charge density is gradually decreased as the wt% of BTO NPs increases [Fig. S5]. The results in Fig. 3(c) also reflect this trend. The output performance is increased until the wt% of BTO NPs in the composite layer reaches 10 wt%. Afterwards, both output voltage and current are continuously lowered. Therefore, there exit optimal conditions to maximize the output performance of TEG by adjusting polarization direction and wt% of BTO NPs inside PDMS. In this work, we also note that adding *tetragonal* phase BTO NPs also increases permittivity as well [Fig. S5]. However, surface dipoles effects play more dominant role in the *tetragonal* phase BTO NPs-PDMS composite TEG"s output performance [Fig. S6].

Using the best performing TEG, we measured the electrical output after connecting loads with different resistances. As shown in Fig. 4(a), the voltage remains close to 0 and the current does not vary significantly when load resistance is below 10 kΩ. As the load resistance is increased from 10 kΩ to 100 MΩ, the voltage (current) across the load rapidly increases (decreases). Thus, the instantaneous power on the load is relatively small when the resistance is below 10 kΩ. The power on the load starts to sharply increase above 100 kΩ and reach the maximum output power (2.5 mW cm^{-2}) at 10 MΩ load resistance [Fig. 4(b)]. The output power of TEG was sufficient to instantaneously light up 250 commercial blue LEDs when the output is connected through a rectifying bridge circuit.

4. Conclusion

In conclusion, we performance enhancement of triboelectric generators (TEGs) by modulating dielectric permittivity and

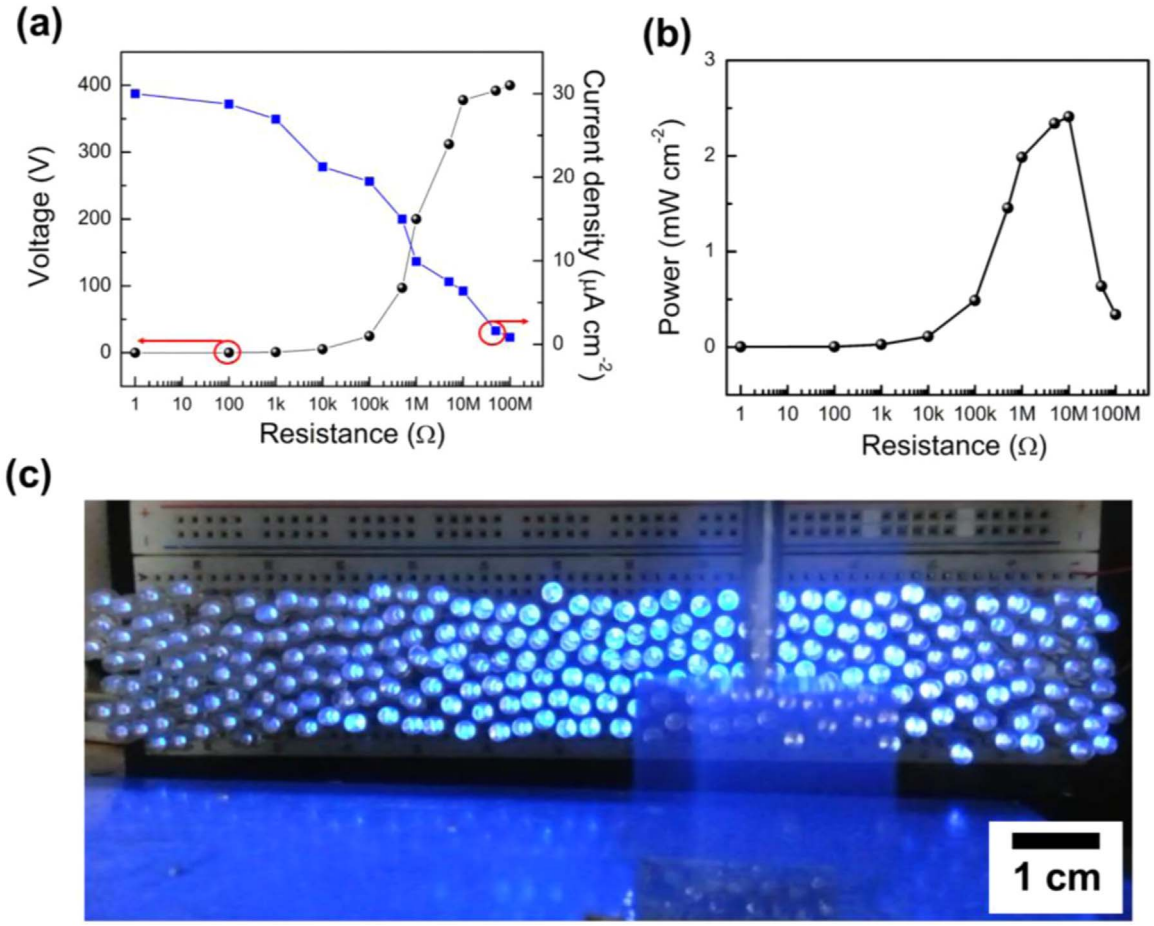

Fig. 4. (a) Voltage and current density plot of the TEG (downward polarized with 10 wt% BTO NPs in the composite thin film) as a function of load resistances. (b) Power density plot as a function of load resistances. The peak output power density was obtained with a 10 MΩ load resistance. (c) Instantaneous lighting of 250 commercial blue LEDs during contact electrification processes.

optimizing the effects from polarized dipoles in the composite thin films, composed of barium titanate nanoparticles (BTO NPs) and polydimethylsiloxane (PDMS). Our results show that peak output power density of the TEGs can be greatly enhanced either by increasing permittivity or aligning polarization domain of the composite layer, exhibiting over 5-fold increases in output power density. In particular, the highest peak output power density was achieved in the dipole-polarized TEG with 50% less inclusion of BTO NPs in the composite layer. The work here provides simple performance enhancement methods and offers an insight into the roles of both permittivity-induced and dipole-moment-induced effects on the electrical output of TEGs.

Acknowledgements

This research was supported by Basic Science Research Program through the National Research Foundation of Korea (NRF-2015R1A1A1A05027235).

Appendix A. Supplementary material

Supplementary data associated with this article can be found in the online version at http://dx.doi.org/10.1016/j.nanoen.2016.05.002.

References

[1] Z. Zhao, X. Pu, C. Du, L. Li, C. Jiang, W. Hu, Z.L. Wang, ACS Nano (2016) 1780–1787.
[2] Y. Yang, G. Zhu, H. Zhang, J. Chen, X. Zhong, Z.-H. Lin, Y. Su, P. Bai, X. Wen, Z. L. Wang, ACS Nano. 7 (2013) 9461–9468.
[3] Y. Xie, S. Wang, L. Lin, Q. Jing, Z.-H. Lin, S. Niu, Z. Wu, Z.L. Wang, ACS Nano 7 (2013) 7119–7125.
[4] Y. Su, X. Wen, G. Zhu, J. Yang, J. Chen, P. Bai, Z. Wu, Y. Jiang, Z.L. Wang, Nano Energy 9 (2014) 186–195.
[5] G. Zhu, Y. Su, P. Bai, J. Chen, Q. Jing, W. Yang, Z.L. Wang, ACS Nano 8 (2014) 6031–6037.
[6] T. Jiang, L.M. Zhang, X. Chen, C.B. Han, W. Tang, C. Zhang, L. Xu, Z.L. Wang, ACS Nano 9 (2015) 12562–12572.
[7] Q. Liang, X. Yan, Y. Gu, K. Zhang, M. Liang, S. Lu, X. Zheng, Y. Zhang, Sci. Rep. 5 (2015) 9080.
[8] S.-B. Jeon, D. Kim, G.-W. Yoon, J.-B. Yoon, Y.-K. Choi, Nano Energy 12 (2015) 636–645.
[9] Z.-H. Lin, G. Cheng, S. Lee, K.C. Pradel, Z.L. Wang, Adv. Mater. 26 (2014) 4690–4696.
[10] P. Bai, G. Zhu, Z.-H. Lin, Q. Jing, J. Chen, G. Zhang, J. Ma, Z.L. Wang, ACS Nano 7 (2013) 3713–3719.
[11] X. Cheng, B. Meng, X. Zhang, M. Han, Z. Su, H. Zhang, Nano Energy 12 (2015) 19–25.
[12] W. Yang, J. Chen, G. Zhu, J. Yang, P. Bai, Y. Su, Q. Jing, X. Cao, Z.L. Wang, ACS Nano 7 (2013) 11317–11324.
[13] S. Wang, L. Lin, Z.L. Wang, Nano Lett. 12 (2012) 6339–6346.
[14] B. Meng, W. Tang, X. Zhang, M. Han, W. Liu, H. Zhang, Nano Energy 2 (2013) 1101–1106.
[15] Y.H. Kwon, S.-H. Shin, J.-Y. Jung, J. Nah, Nanotechnology 27 (2016) 205401.
[16] F.-R. Fan, L. Lin, G. Zhu, W. Wu, R. Zhang, Z.L. Wang, Nano Lett. 12 (2012) 3109–3114.
[17] G. Zhu, C. Pan, W. Guo, C.-Y. Chen, Y. Zhou, R. Yu, Z.L. Wang, Nano Lett. 12 (2012) 4960–4965.
[18] S.-J. Park, M.-L. Seol, S.-B. Jeon, D. Kim, D. Lee, Y.-K. Choi, Sci. Rep. 5 (2015) 13866.

[19] B. Dudem, Y.H. Ko, J.W. Leem, S.H. Lee, J.S. Yu, ACS Appl. Mater. Interfaces 7 (2015) 20520–20529.
[20] D. Kim, S.-B. Jeon, J.Y. Kim, M.-L. Seol, S.O. Kim, Y.-K. Choi, Nano Energy 12 (2015) 331–338.
[21] S.-H. Shin, Y.H. Kwon, Y.-H. Kim, J.-Y. Jung, M.H. Lee, J. Nah, ACS Nano 9 (2015) 4621–4627.
[22] P. Bai, G. Zhu, Y.S. Zhou, S. Wang, J. Ma, G. Zhang, Z.L. Wang, Nano Res. 7 (2014) 990–997.
[23] Y. Yang, H. Zhang, J. Chen, S. Lee, T.-C. Hou, Z.L. Wang, Energy Environ. Sci. 6 (2013) 1744–1749.
[24] J. Chen, H. Guo, X. He, G. Liu, Y. Xi, H. Shi, C. Hu, ACS Appl. Mater. Interfaces 8 (2016) 736–744.
[25] A. Li, C. Ge, P. Lu, D. Wu, S. Xiong, N. Ming, Appl. Phys. Lett. 70 (1997) 1616–1618.
[26] H.-W. Lee, S. Moon, C.-H. Choi, D.K. Kim, J. Am. Ceram. Soc. 95 (2012) 2429–2434.
[27] S. Niu, S. Wang, L. Lin, Y. Liu, Y.S. Zhou, Y. Hu, Z.L. Wang, Energy Environ. Sci. 6 (2013) 3576–3583.

Yang Hyeog Kwon received his B.S. degree in Department of Electrical Engineering from Chungnam National University, Korea in 2015. He is currently Master course student supervised by Professor Junghyo Nah. His research topic is piezoelectric and triboelectric nanogenerators and self-powered energy storage devices.

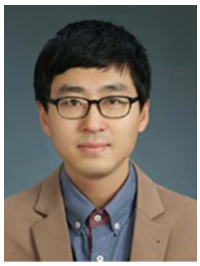

Sung-Ho Shin received his B.S. and M.S. degrees in Department of Electrical Engineering from Chungnam National University, Korea in 2013 and 2015, respectively. He is currently pH.D. course student supervised by Professor Junghyo Nah. His research topic includes piezoelectric & triboelectric nanogenerators, piezoelectric water splitting, and hybrid energy harvesting devices.

Joo-Yun Jung received his PhD in 2010 from the department of electrical and computer engineering, University of Texas at Austin. He joined KIMM (Korea Institute of Machinery and Materials) in Daejeon, South Korea, in 2010. At present, he is a senior researcher in KIMM. His research interests include nanoimprint, metamaterials and nanostructures-based photonic, and plasmonic applications.

Min Hyung Lee received his pH.D. in material chemistry from Northwestern University in 2010 under advice of Prof. Teri W. Odom. He performed postdoctoral researches from 2010 to 12 in EECS, UC Berkeley and LBNL with Prof. Ali Javey and Dr. Joel Ager. Since 2012, he joined as a faculty at Dept. of Applied Chemistry at Kyung Hee University, Korea. His researches have focused on developing new type of nanostructures and using in plasmonics, solar-to-fuel conversion, and nanogenerator applications.

Junghyo Nah received pH.D. in Electrical and Computer Engineering from the University of Texas at Austin in 2010. He worked as a postdoctoral scholar at University of California at Berkeley from 2011 to 2012. He joined the faculty of the Department of Electrical Engineering, Chungnam National University, Daejeon, Korea, in 2012. He is now an associate professor at this university. His research interests include piezoelectric and triboelectric energy harvesting devices, flexible electronics, and high performance transistors using low dimensional semiconductor nanomaterials.